UDK 669.715: 552.123
Original scientific article/Izvirni znanstveni članek

ISSN 1580-2949
MTAEC9, 56(3)289(2022)

EFFECT OF INCLUSIONS ON THE SOFTENING MECHANISM OF Al 1235 ALLOY DURING THERMAL DEFORMATION

VPLIV VKLJUČKOV NA MEHANIZEM MEHČANJA ZLITINE VRSTE Al 1235 MED TERMIČNO DEFORMACIJO

Wenduan Yan[1], Gaosheng Fu[2*], Hao Huang[1], Mingdeng Zhong[1]

[1]Minnan University of Science and Technology, Quanzhou 362700, China
[2]Fuzhou University, Fuzhou 350108, China

Prejem rokopisa – received: 2022-03-15; sprejem za objavo – accepted for publication: 2022-04-06

doi:10.17222/mit.2022.448

The effect of inclusions on the softening mechanism of a pure aluminum alloy is studied with TEM, EDAX and SAED. Oxide inclusions and iron-rich second-phase particles are the main inclusions in Al 1235 alloy. The phase of iron-rich particles in the alloy is phase $AlFe_3$ with a lattice constant of 5.79 and crystal band axis of [231]. During thermal deformation, coarser inclusions in the alloy are beneficial to the nucleation of dynamic recrystallization, but they have a great effect on the separation of the alloy matrix. Nucleation and growth of dynamic-recrystallization grains are restricted by finer inclusions, reducing the possibility of aluminum-matrix fracture. The preferred places for dynamic-recrystallization nucleation include boundaries at the intersection of three grains, the dislocation plug area, the surface of the coarse oxide inclusions or the coarse second-phase inclusions.

Keywords: Al 1235 alloy, TEM, softening mechanism, oxide inclusions, second-phase particles

V pričujočem članku avtorji predstavljajo raziskavo vpliva vključkov na mehanizem mehčanja zlitine vrste Al 1235. Raziskavo so izvajali s pomočjo presevnega elektronskega mikroskopa (TEM), rentgenske energijske disperzijske spektroskopije (EDAX), in elektronske difrakcije na specifičnem preseku (SAED). V matrici zlitine Al 1235 so prisotni v glavnem oksidni vključki in na železu bogati delci sekundarne faze $AlFe_3$ z mrežno konstanto 5,79 in osjo kristalnega pasu [231]. Med termično deformacijo imajo bolj grobi vključki v zlitini pozitiven vpliv na nukleacijo dinamične rekristalizacije toda imajo velik vpliv na ločevanje matrice v zlitini. Nukleacijo in rast kristalnih zrn med dinamično rekristalizacijo omejujejo finejši vključki, kar zmanjša možnost porušitve kovinske matrice. Prednostna mesta za nukleacijo kristalnih zrn med dinamično rekristalizacijo so kristalne meje na preseku treh zrn, področja dislokacijskih klinov in površina grobih oksidnih vključkov ali grobih delcev sekundarne faze.

Ključne besede: zlitina Al 1235, TEM, mehanizem mehčanja, oksidni vključki, delci sekundarne faze

1 INTRODUCTION

Aluminum foil is a kind of flexible metal which is made by repeatedly rolling commercial pure aluminum. Al 1235 alloy is mainly used for aluminum foil containers and cooking bags, which are innocuous, healthy, highly flexible, moisture resistant, etc.[1–3] Melt purification is the key to improving the metallurgical qualities and forming properties of Al 1235 alloy; therefore, such a treatment affects the mechanical behavior during thermal deformation. Inclusion is the key factor throughout the process.[4,5] Inclusions have some adverse effects on the foil quality, such as the formation of pinholes or cracks, and may even make aluminum foil fracture.

The thermal-deformation behavior of a pure-aluminum alloy is a complex combination of work hardening and dynamic-recrystallization softening.[6–8] Little research on the complicated thermo-softening mechanism of aluminum alloys has been conducted due to their poor flowability, sensitivity to temperature, strain rate, and inclusions.[9–11] A behavior study of the inclusions in the softening of a thermally deformed Al 1235 alloy is important for optimizing the processing performance and controlling the internal microstructure evolution of a pure-aluminum alloy during deformation.

*Corresponding author's e-mail:
fugaosheng@fzu.edu.cn (Gaosheng Fu)

2 EXPERIMENTAL PART

As a pure aluminum alloy, Al 1235 alloy with a 99.35 *w*/% Al content was chosen in this study.[12–14] The chemical composition (in mass fractions, *w*/%) is listed in **Table 1**. The metal was melted with conventional purification, and the percentage of inclusions tested with flux irrigation was 0.082 *w*/%.

Ingots were processed with homogenizing annealing at the conditions including an annealing temperature of 560 °C, holding time of 13 h and air-cooling.[12] Isothermal axisymmetric compression tests were carried out in a Geeble-1500 dynamic thermal/mechanical simulation machine at a deformation temperature of 300–500 °C, strain rate of 0.1–10 s^{-1} and deflection of 50 %. Deformed specimens were quenched in water quickly after each compression test in order to maintain the microstructure.

Table 1: Chemical composition of Al 1235 alloy

Element	Si	Fe	Cu	Mn	Mg	Ni	Zn	Ti	Al
composition (*w*/%)	0.095	0.38	0.002	0.002	0.0001	0.0001	0.006	0.015	Bal.

Hot-deformed specimens were cut in the longitudinal direction parallel to the compression direction with WEDM using DK7255 and processed into thin slices. The samples were etched after grinding and mechanical polishing. The microstructure was observed with an XJG-05 horizontal metallographic polarizing microscope. After grinding and mechanical polishing, the thin slices with a thickness between 0.1 mm and 0.2 mm were made into film samples with a MTP-1A magnetic-drive double-jet thinning device, and the film samples were not penetrated. The electrolyte in the device was composed of 5 % $HClO_3$ and 95 % ethyl alcohol. Transmission electron microscopy (TEM), energy dispersive X-ray analysis (EDAX) and selected area electron diffraction (SAED) carried out with a Tecnai F20 field-emission transmission electron microscope were used.

3 RESULTS AND DISCUSSION

3.1 Microstructure of Al 1235 alloy before deformation

Figure 1 shows the microstructure of Al 1235 alloy before deformation. On the figure, inclusions in the pure aluminum alloy are obvious. Coarse inclusions in the alloy dispersed. A few tiny inclusions can be seen in the conventionally purified metal. The average size of inclusions was assessed with quantitative metallography (the linear intercept method) within a metallographic analysis, and the average size of inclusions was 25.3 μm.

3.2 Effect of oxide inclusions on the thermal softening mechanism

Insoluble inclusions in an aluminum alloy are mainly oxide inclusions.[15,16] By analyzing the microstructure of the thermally deformed Al 1235 alloy, the influences of the inclusion content and shape (size, etc.) on the thermal-deformation behavior of Al 1235 alloy can be determined. **Figures 2** and **3** show TEM images of the inclusions and EDAX results for the thermally deformed Al 1235 alloy.

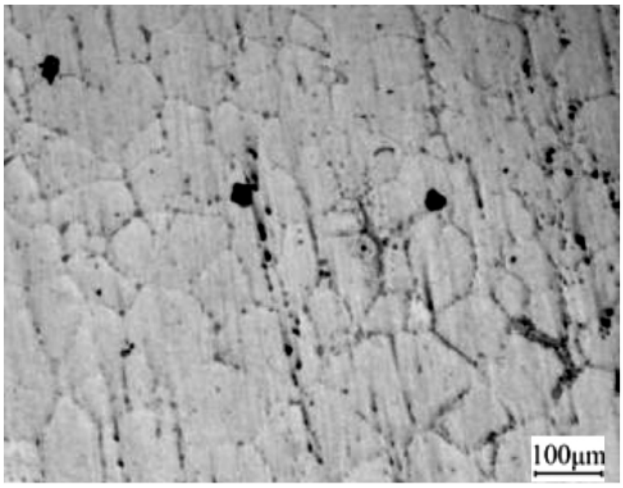

Figure 1: Microstructure of Al 1235 alloy before deformation

On **Figures 2b** and **3b**, the oxide inclusions are mainly Al_2O_3 with some iron-rich inclusions. **Figure 4** shows TEM images of coarse inclusions in deformed Al 1235 alloy. On **Figure 4**, the dislocation density around larger inclusions is very low, dislocation-bundle sets form clear, flat and large-angle grain boundaries, and the dynamic recrystallization is relatively complete. This is because the deformation of the lattice caused by large inclusions forms a large degree of lattice distortion. The

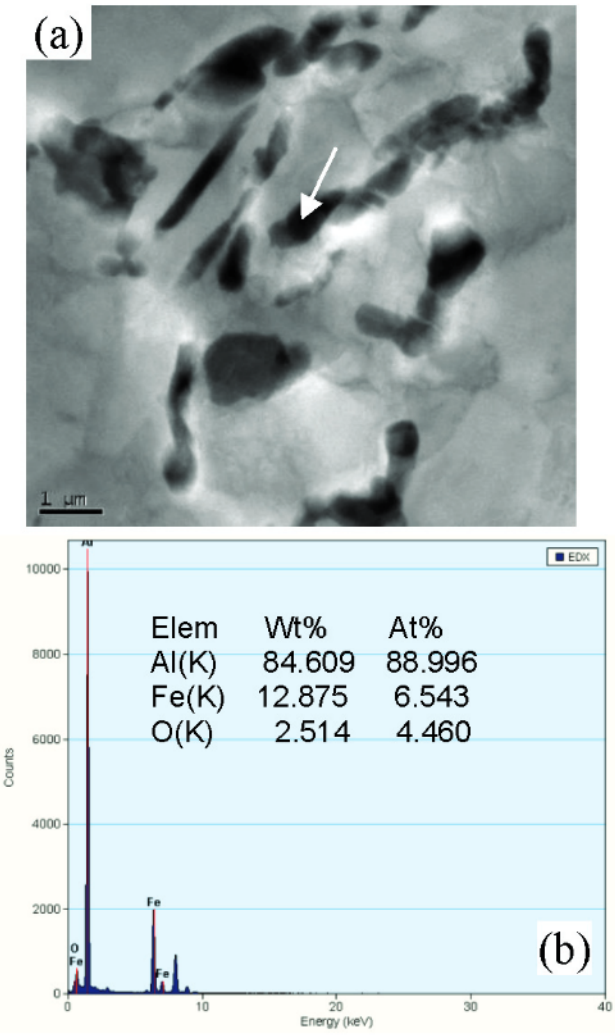

Figure 2: Al 1235 alloy deformed at 400 °C and 1 s^{-1}: a) TEM image of inclusions, b) EDAX results for the arrowed location from **Figure 2a**

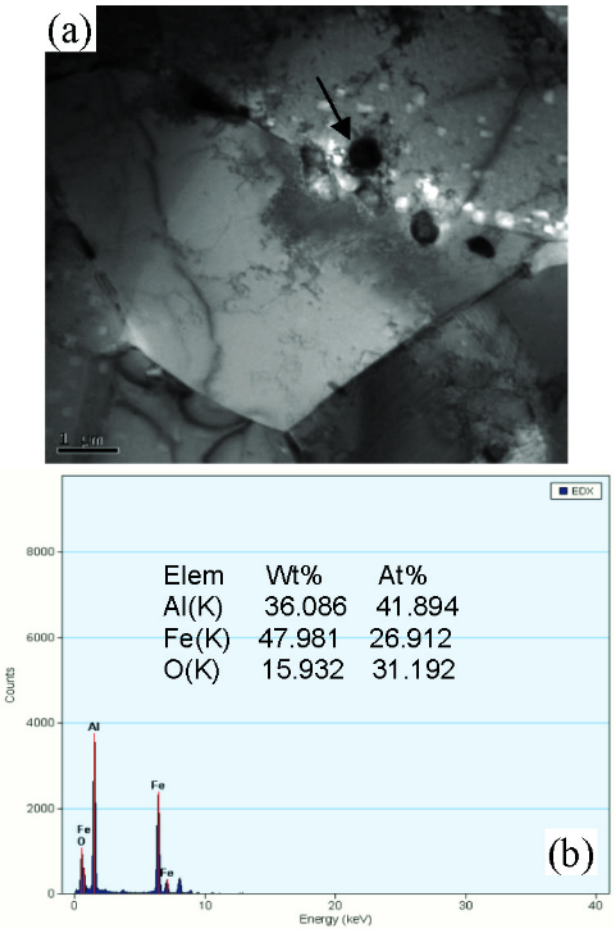

Figure 3: Al 1235 alloy deformed at 500 °C and 1 s^{-1}: a) TEM image of inclusions, b) EDAX results for the arrowed location from **Figure 3a**

released energy of lattice distortion can make the deformation storage energy larger, providing favorable energy conditions for dynamic-recrystallization nucleation and making the coarse inclusions become the core of recrystallization. Therefore, the existence of these large oxide inclusions is conducive to the nucleation of dynamic recrystallization.

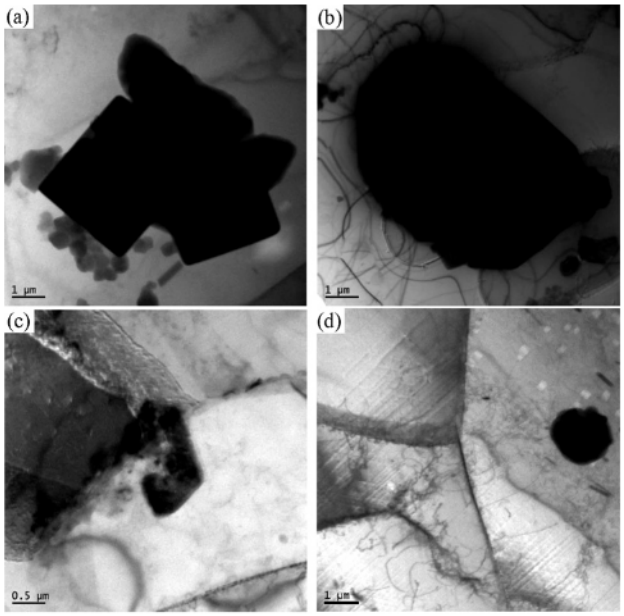

Figure 4: TEM images of coarse inclusions in Al 1235 alloy deformed at: a) 400 °C and 1 s^{-1}, b) 400 °C and 10 s^{-1}, c) 400 °C and 0.1 s^{-1}, d) 500 °C and 0.1 s^{-1}

Figure 5 shows some fine inclusions in the deformed Al 1235 alloy. The entanglement of dislocation lines around the small inclusions can be seen from the figure. It is obvious that the dislocation movement is hindered by fine inclusions, playing a role in dislocation pinning. As a result, the resistance of subgrain boundary migration is increased, and the formation and growth of dynamically recrystallized grains are hampered.

It can be further seen from **Figure 6** that small inclusions have a pinning effect on the dislocation movement, thus hindering the progress of dynamic recrystallization. In addition, fine inclusions tend to disperse during deformation at low strain rates as shown in **Figures 6a** and **6b**, but they tend to aggregate at high strain rates as shown in **Figure 6c**.

Nevertheless, the morphology of inclusions has a great influence on the thermal-deformation behavior of

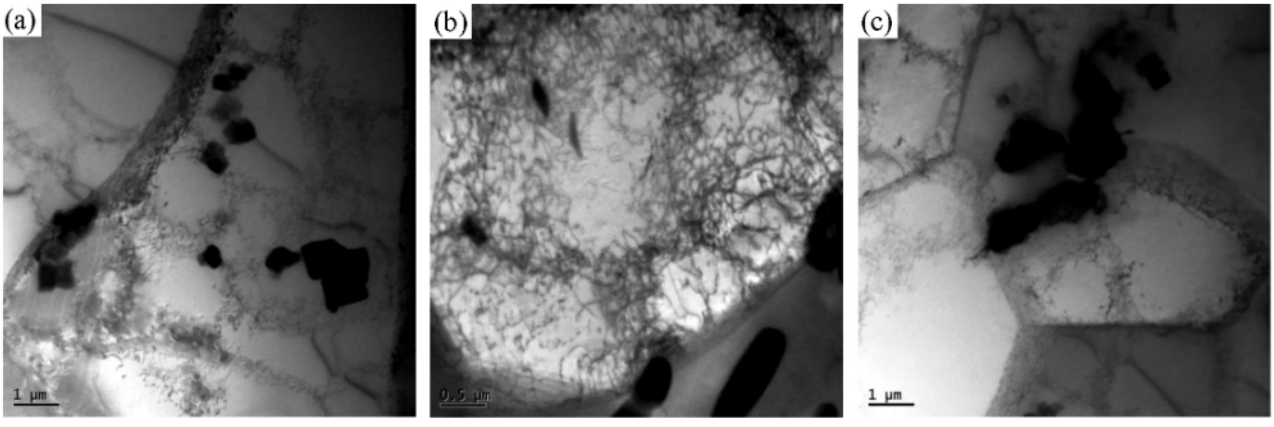

Figure 5: TEM images of fine inclusions in Al 1235 alloy deformed at 0.1 s^{-1} and a temperature: a) 300 °C, b) 400 °C, c) 500 °C

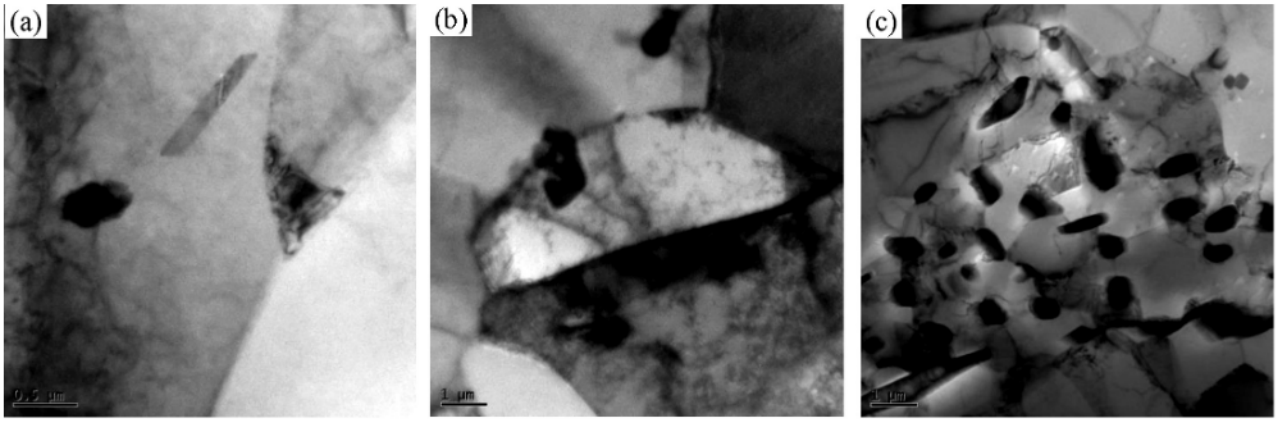

Figure 6: TEM images of fine inclusions in Al 1235 alloy deformed at 400 °C and deformed at: a) 0.1 s^{-1}, b) 1 s^{-1}, c) 50 s^{-1}

the aluminum matrix. The dispersed flaky inclusions have a big effect on the fragmentation of the metal matrix, as seen in **Figure 3**. On the contrary, the fragmentation possibility of the matrix is reduced by some oxide inclusions that are small and round.

3.3 Effect of second-phase particles on the thermal softening mechanism

The main elements of Al 1235 alloy are Fe and Si, as shown in **Table 1**. Phase Al-Fe is the main binary compound, and phase Al_3Fe is its equilibrium phase. Due to non-equilibrium solidification, phase Al-Fe usually ex-

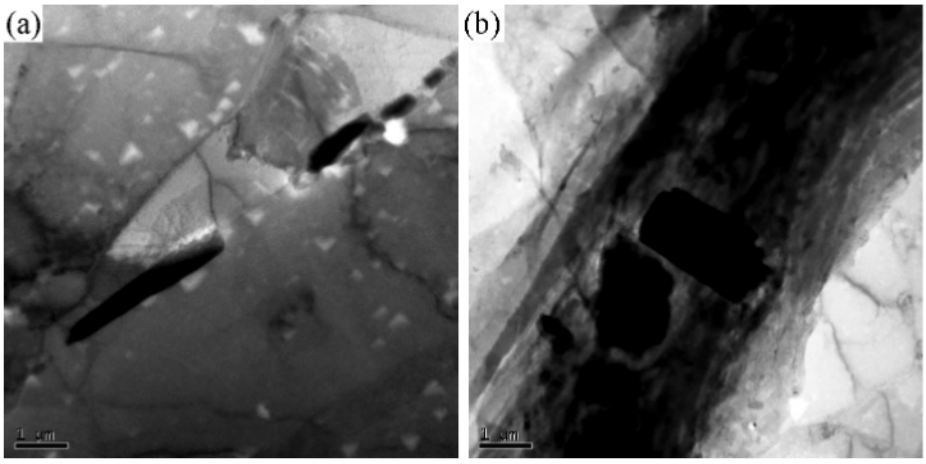

Figure 7: Second-phase particles of Al 1235 alloy deformed at 400 °C: a) 0.1 s^{-1}, b) 1 s^{-1}

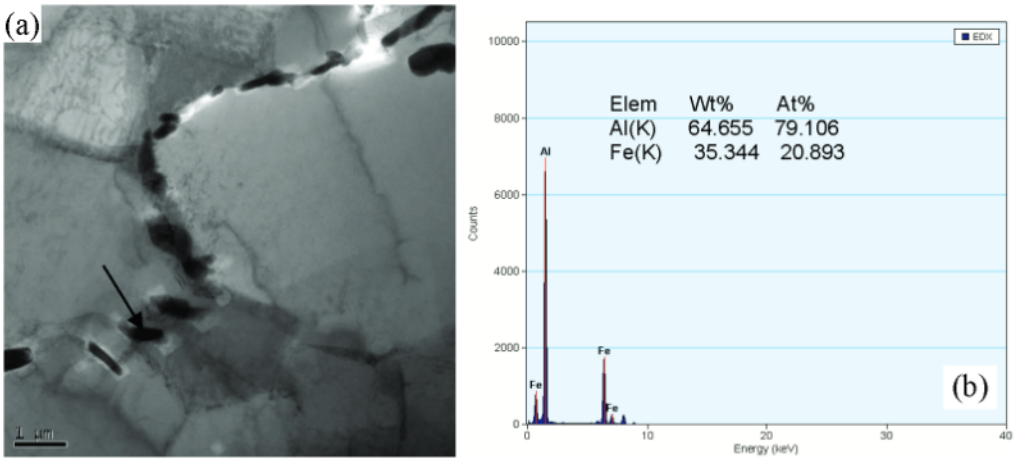

Figure 8: Second-phase particles of Al 1235 alloy: a) deformed at 450 °C and 0.1 s^{-1}, b) EDAX of the arrowed location from **Figure 8a**

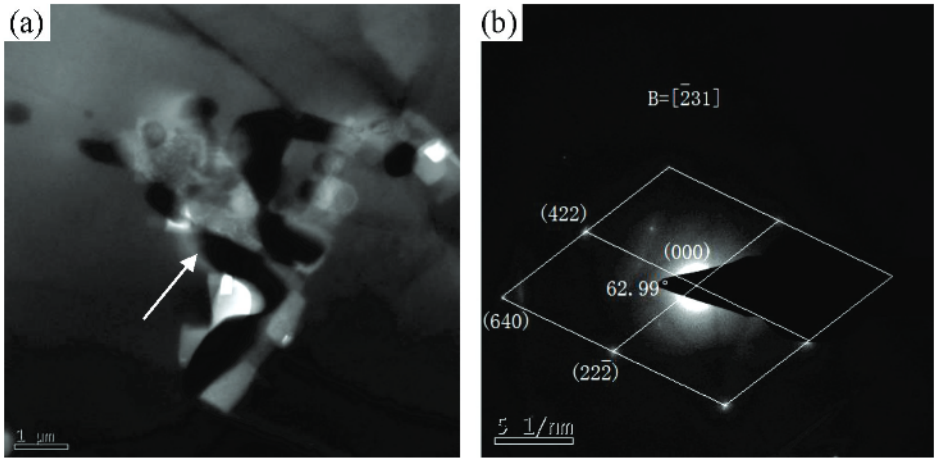

Figure 9: Al 1235 alloy deformed at 400 °C and 10 s^{-1}: a) the shape of second-phase particles, b) SAED of the arrowed location from **Figure 9a**

ists in the form of a non-equilibrium phase.[17,18] However, the non-equilibrium phase is generally transformed into equilibrium phase Al_3Fe during the homogenization of the alloy. **Figures 7** and **8** show the typical morphology of the long needle-like second-phase particles of Al 1235 alloy, and a semi-quantitative analysis of its energy spectrum, respectively.

Figure 9 shows the second-phase particles and SAED results of deformed Al 1235 alloy. According to the calibration results of selected area electron diffraction, the lattice constant *a* is 5.79, which is close to the $AlFe_3$ lattice constant, which is 5.82. It can be assumed that the second phase is the iron-rich precipitate phase with a cubic structure, which is phase $AlFe_3$, and the crystal band axis is [$\bar{2}$31].

According to SEM, the morphology of the second-phase particles of the thermally deformed Al 1235 alloy mainly exhibits a long needle-like shape and a short rod-like shape. According to the precipitation location, the second-phase particles in Al 1235 alloy mainly exist in the grain boundaries or in the grains. After thermal deformation, the coarse and long needle-like second-phase particles at grain boundaries of Al 1235 alloy are crushed, and a few second-phase particles at grain boundaries obtain a bone-like shape. However, the second-phase particles in the grains mainly have a globular shape or a short bone-like shape. These particles are highly dispersed. They have a big dispersion-strengthening effect on the aluminum matrix, as shown in **Figure 10**.

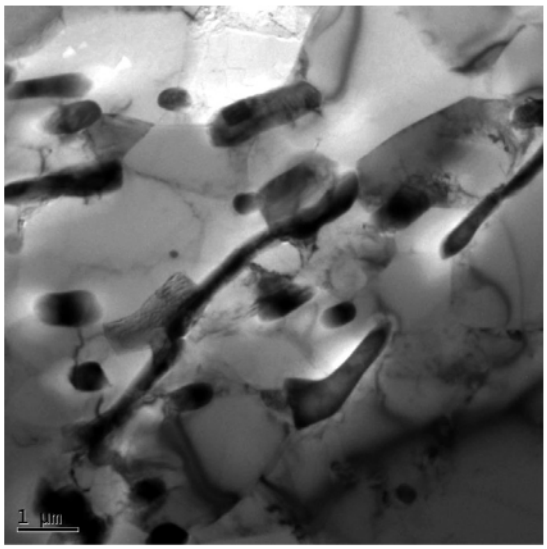

Figure 10: Second-phase particles of Al 1235 alloy deformed at 400 °C and 50 s^{-1}

Due to the difference in the precipitation location and morphology, the second-phase particles have different effects on the dynamic-softening behavior of the alloy. The coarse second-phase particles at the grain boundaries act like coarse insoluble inclusions, and the phase interface can also become a non-spontaneous nucleation base for recrystallization. There is obvious dislocation entanglement around the dispersed fine second-phase particles in the grains, and these regions with high dislocation density provide favorable conditions for dynamic recrystallization.

There are two reasons for the favorable dynamic recrystallization caused by second-phase particles in the alloy.[14–18] Firstly, second-phase particles become obstacles to the dislocation movement during thermal deformation. In the meantime, the particles can pin dislocation and increase dislocation slip and uneven dislocation distribution. As a result, the breeding period of recrystallization nucleation is shortened and the nucleation rate N is increased. Secondly, these particles can block the interface migration, including small-angle boundaries or large-angle grain boundaries and hinder the growth of crystal nuclei at the same time. As a result, the growth rate of recrystallized grains G is reduced, and some fine equiaxed grains are obtained.

4 CONCLUSIONS

1) The main inclusions in Al 1235 alloy are oxide inclusions and iron-rich second-phase particles.

2) The structure of iron-rich second-phase particles in the alloy is cubic, with a lattice constant of 5.79 and crystal band axis of $[\bar{2}31]$. The second phase is $AlFe_3$.

3) The dynamic-softening behavior of Al 1235 alloy is affected by oxide inclusions and iron-rich second-phase particles. Dispersed flaky inclusions have a big effect on the fragmentation of the metal matrix. The possibility of matrix fragmentation is reduced by some oxide inclusions which are small and round.

4) The primary grain boundaries at the intersection of three grains, dislocation plug area, external surface of the coarse oxide inclusions, or coarse second-phase inclusions can be the preferred place for dynamic-recrystallization nucleation.

Acknowledgements

The authors acknowledge with gratitude the financial support received from the Natural Science Foundation of Fujian Province (No. 2021J01530), China.

5 REFERENCES

[1] H. Song, W. H. Hao, X. W. Mu, F. Q. Zhao, X. X. Hao, G. H. Geng, Effect of pulse current on the wear behavior of a cold-rolled commercially pure aluminum sheet, Strength of Materials, 53 (**2021**) 5, 376–386, doi:10.1007/s11223-021-00257-3

[2] K. Kondoh, J. Umeda, H. Sannomiya, Interfacial reaction behavior and mechanical properties of pure aluminum and magnesium alloy dissimilar materials fabricated by hot press and heat treatment, Materials Characterization, 157 (**2019**), 109879, doi:10.1016/j.matchar.2019.109879

[3] H. R. Ammar, The impact of alloying elements addition on the flow behavior of aluminum alloys, Transactions of the Indian Institute of Metals, 73 (**2020**) 6, 1605–1609, doi:10.1007/s12666-020-01935-7

[4] R. Kumar, A. Gupta, T. R. Dandekar, R. K. Khatikar, Evolution of microstructure and texture during homogenization in a strip cast AA8011 aluminum alloy, Intermetallics, 130 (**2021**), 107064, doi:10.1016/j.intermet.2020.107064

[5] Q. Y. Yang, Y. L. Zhou, Y. B. Tan, Effects of microstructure, texture evolution and strengthening mechanisms on mechanical properties of 3003 aluminum alloy during cryogenic rolling, Journal of Alloys and Compounds, 884 (**2021**) 1, 161135, doi:10.1016/j.jallcom.2021.161135

[6] A. A. Tiamiyu, A. Y. Badmos, A. G. Odeshi, J. A. Szpunar, The influence of temper condition on adiabatic shear failure of AA 2024 aluminum alloy, Materials Science and Engineering A, 708 (**2017**), 492–502, doi:10.1016/j.msea.2017.10.026

[7] J. Li, F. Li, Y. An, Characterization of hot deformation behavior for pure aluminum using 3D processing maps, High Temperature Materials Process, 37 (**2018**), 9–10, doi:10.1515/htmp-2017-0078

[8] T. Sakai, A. Belyakov, R. Kaibyshev, H. Miura, J. J. Jonas, Dynamic and post-dynamic recrystallization under hot, cold and severe plastic deformation conditions, Progress in Materials Science, 60 (**2014**) 1, 130–207, doi:10.1016/j.pmatsci.2013.09.002

[9] M. Härtel, B. Bohne, M. Wagner, Microstructural evolution during tension-compression in-plane deformation of a pure aluminum sheet, IOP Conference Series: Materials Science and Engineering, 181 (**2017**) 1, 12–14, doi.org/10.1088/1757-899X/181/1/012024

[10] K. T. Son, M. H. Kim, S. W. Kim, Evaluation of hot deformation characteristics in modified AA5052 using processing map and activation energy map under deformation heating, Journal of Alloys and Compounds, 740 (**2018**), 96–108, doi.org/10.1016/j.jallcom.2017.12.357

[11] Y. V. Gamin, T. K. Akopyan, A. N. Koshmin, Microstructure evolution and property analysis of commercial pure Al alloy processed by radial-shear rolling, Archives of Civil and Mechanical Engineering, 20 (**2020**) 4, 00143, doi:10.1007/s43452-020-00143-w

[12] W. D. Yan, G. S. Fu, H. L. Chen, G. Q. Chen, Effects of oxide inclusions on flow stress behavior of 1235 aluminum alloy during hot compression, Journal of Materials Engineering and Performance, 21 (**2012**) 10, 2203–2206, doi:10.1007/s11665-012-0152-0

[13] G. Q. Chen, G. S. Fu, T. Y. Wei, C. Z. Cheng, J. D. Wang, H. S. Wang, Establishment of dynamic-recrystallization-state diagram for hot deformation of 3003 aluminum alloy, Materials and Technology, 52 (**2018**) 3, 341–347, doi:10.17222/mit.2017.176

[14] W. D. Yan, G. S. Fu, H. L. Chen, L. L. Song, W. Liu, Texture characteristics of Al 1235 alloy during rolling, Materials and Technology, 53 (**2019**) 6, 821–825, doi:10.17222/mit.2018.195

[15] Y. L. Ma, Y. C. Huang, X. Zhang, Precipitation thermodynamics and kinetics of the second phase of Al-Zn-Mg-Cu-Sc-Zr-Ti aluminum alloy, Journal of Materials Research and Technology, 10 (**2020**), 445–452, doi:10.1016/j.jmrt.2020.11.075

[16] W. D. Yan, G. S. Fu, Y. H. Xu, W. Q. Lai, H. L. Chen, Effect of Sr addition on the microstructure and properties of the A356 Al alloy, Mater. Tehnol., 55 (**2021**) 3, 109–114, doi:10.17222/ mit2020.038

[17] C. Zhang, C. Wang, Q. Zhang, Influence of extrusion parameters on microstructure, texture, and second-phase particles in an Al-Mg-Si alloy, Journal of Materials Processing Technology, 270 (**2019**), 323–334, doi:10.1016/j.jmatprotec.2019.03.014

[18] B. Wang, Y. Yi, H. He, Effects of deformation temperature on second-phase particles and mechanical properties of multidirectionally-forged 2A14 aluminum alloy, Journal of Alloys and Compounds, 871 (**2021**), 159459, doi:10.1016/j.jallcom.2021.159459